CHEMISTRY
A European Journal

Supporting Information

Enhancement of the Photocatalytic Activity of Carbon Nitrides by Complex Templating

Zu Peng Chen, Markus Antonietti, and Dariya Dontsova*[a]

chem_201500579_sm_miscellaneous_information.pdf

Supporting Information

Materials. Melamine (99 %), aluminium nitrate nonahydrate (98 %), Rhodamine B (95 %), hexachloroplatinic acid (H_2PtCl_6) solution (8 wt. % aqueous solution) were purchased from Sigma Aldrich, and triethanolamine (TEOA, 98 %) was purchased from Alfa Aesar. All chemicals were of analytical grade and used without further purification. The rate and extent of complex formation discussed in this paper are highly dependent on quality of melamine used (purity, crystallinity and particle size), and may be different for different batches of the precursor, even if the provider is the same.

Rhodamine B photodegradation. The photodegradation experiments were performed using a 30 W blue LED module (OSA Opto Lights) emitting at 465 nm, or 50 W white LED array (Bridgelux BXRA-50C5300, $\lambda > 410$ nm). In brief, 5 mg of catalyst were dispersed in 5 mL of 20 mg/L RhB aqueous solution, followed by sonication for 5 minutes. The suspension was stirred for 0.5 - 2 hours in dark to reach the dark-adsorption equilibrium, followed by irradiation with an LED module from a fixed distance of 5 cm. 300 µL of suspension were taken at a given time *t*, and then diluted to 2 mL with deionized water, kept for 120 minutes in a dark to allow catalyst precipitation. The suspension was then analyzed by T70 UV-Vis spectrophotometer to monitor the RhB concentration change. To quantitatively estimate the catalytic activity, we used the first-order kinetic model to fit the degradation data:

$$\ln(C_0/C)=k\cdot t, \qquad \text{Eq. 1}$$

where C_0 and C indicate the initial (after 30 minutes dark equilibration; $t=t_0$) and residual after the irradiation time t concentrations of RhB, and the rate constant k reflects the photoactivity of the catalysts.

Photocatalytic hydrogen evolution tests. Reactions were performed using a side-irradiated closed steel reactor equipped with a Teflon inlet, thermocouple, pressure sensor, magnetic stirring and thermostat, and connected to a Schlenk line. H_2 production was carried out using 50 mg of catalyst dispersed in 38 mL of solvent mixture composed of triethanolamine (TEOA) and water in the ratio of 1/9 (v/v). Pt nanoparticles were deposited on carbon nitrides by in-situ photodeposition procedure using hexachloroplatinic acid (H_2PtCl_6) solution as a precursor. The build-up of H_2 pressure was monitored as a function of the irradiation time. The irradiation source used here is a 50 W white LED array. To confirm that the evolved gas is hydrogen, the headspace of the reactor was analyzed by mass

spectrometry (Pfeiffer Vacuum ThermoStar GSD 301 T gas analyzing system; using argon as carrier gas) after the test. The detailed description of the setup and the test procedure can be found in previous publications [S1].

Characterization. Powder X-Ray diffraction patterns were measured on a Bruker D8 Advance diffractometer with $Cu_{K\alpha}$ radiation (λ = 0.15418 nm) equipped with a scintillation counter detector applying a step size of 2θ = 0.05° and counting time of 3s per step. FT-IR spectra were recorded on a Varian1000 FT-IR spectrometer equipped with an attenuated total reflection unit with diamond applying a resolution of 4 cm^{-1}. Nitrogen adsorption/desorption measurements were performed after degassing the samples at 150 °C for 20 hours using a Quantachrome Quadrasorb SI-MP porosimeter at 77.4 K. N_2 adsorption/desorption isotherms at 77 K were conducted on a Quantachrome Autosorb-1MP instrument after prior degassing. The specific surface areas were calculated by applying the Brunauer-Emmett-Teller (BET) model to adsorption isotherms (N_2 at 77.4 K) for $0.05 < p/p_0 < 0.3$ using the QuadraWin 5.05 software package. The pore size distribution was calculated by the nonlocal density functional theory method (NLDFT). Elemental analysis was accomplished as combustion analysis using a Vario Micro device. SEM images were obtained on a LEO 1550-Gemini microscope. Optical absorbance spectra of powders were measured on a Shimadzu UV 2600 equipped with an integrating sphere. The absorption spectra of RhB solutions were recorded on a T70 UV/VIS spectrophotometer (PG instruments Ltd.). The emission spectra were recorded on LS-50B, Perkin Elmer instrument. The excitation wavelength was 350 nm. EDX investigations were conducted on a Link ISIS-300 system (Oxford Microanalysis Group) equipped with a Si(Li) detector and an energy resolution of 133 eV. Elemental composition of products and chemical states of the surface elements were analyzed by X-ray photoelectron spectroscopy using ESCALab220i-XL electron spectrometer from VG Scientific and 300W AlKα radiation. All binding energies were referenced to the C1s peak at 284.8 eV arising from surface or possible adventitious hydrocarbons. Prior to peak deconvolution, X-ray satellites and inelastic background (Shirley-type) were subtracted for all the spectra.

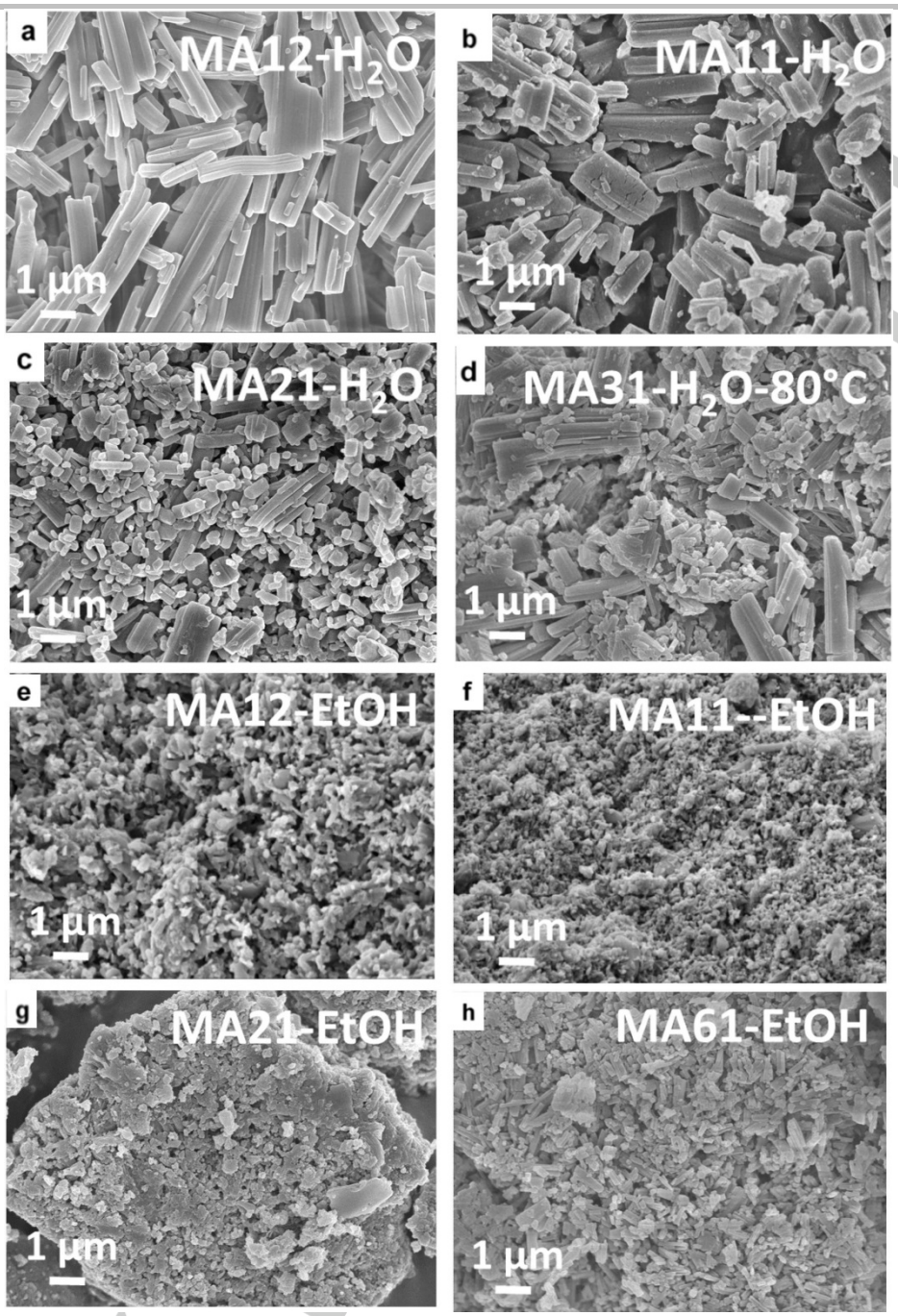

Figure S1. SEM images of MA-complexes prepared using different solvents and reagent ratios.

Table S1. Elemental composition of products and reference g-C_3N_4 according to EA data.

Entry	Product name	C, wt.%	N, wt.%	H, wt.%	C/N weight ratio
1	g-C_3N_4	34.9	60.5	2.00	0.58
2	MA12-H_2O-C_3N_4	30.8	52.1	2.91	0.59
3	MA23-H_2O-C_3N_4	31.2	52.7	2.84	0.59
4	MA11-H_2O-C_3N_4	31.3	53.6	2.82	0.58
5	MA21-H_2O-C_3N_4	30.8	52.4	2.82	0.59
6	MA31-H_2O-C_3N_4	30.6	51.8	2.88	0.59
7	MA31-H_2O-60°C-C_3N_4	28.9	48.9	2.68	0.59
8	MA31-H_2O-80°C-C_3N_4	30.5	51.5	2.72	0.59
9	MA31-H_2O-gel-C_3N_4	30.6	52.3	2.87	0.58
10	MA12-EtOH-C_3N_4	31.5	53,7	2.78	0.59
11	MA23-EtOH-C_3N_4	31.1	53.1	2.71	0.59
12	MA11-EtOH-C_3N_4	31.8	53.6	2.86	0.59
13	MA21-EtOH-C_3N_4	32.7	55.6	2.63	0.59
14	MA31-EtOH-C_3N_4	30.9	52.4	2.93	0.59
15	MA61-EtOH-C_3N_4	31.2	52.2	2.81	0.60
16	MA21-EtOH-top-C_3N_4	30.4	51.7	3.01	0.59
17	MA31-EtOH-top-C_3N_4	30.5	51.8	3.20	0.59
18	MA61-EtOH-top-C_3N_4	31.6	53.4	2.79	0.59

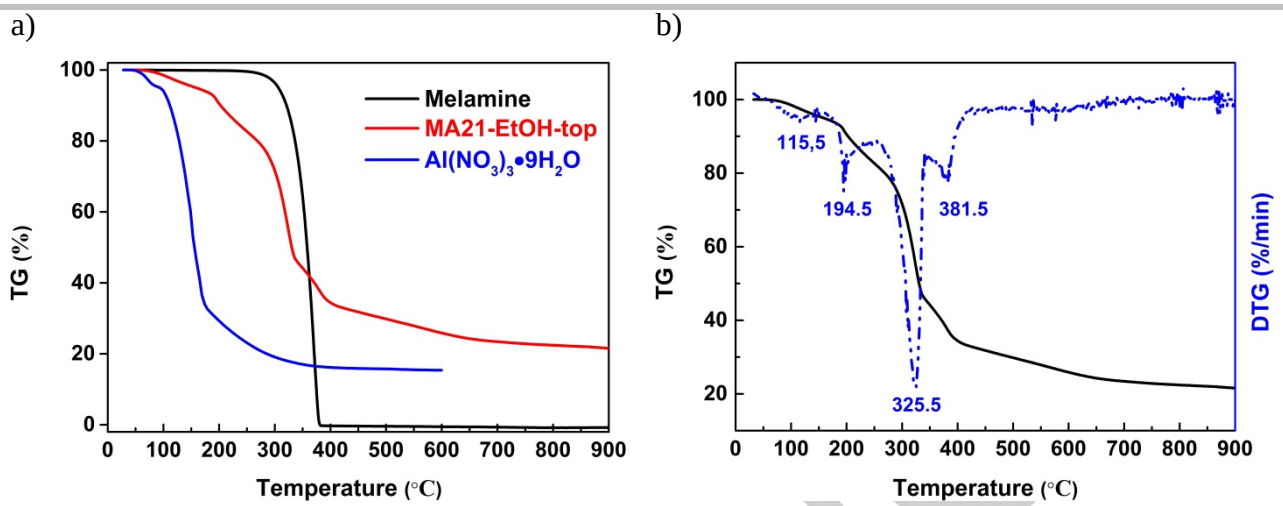

Figure S2. a) TGA curves of pure precursors and of the complex whose composition was the closest to the theoretical one of 3:1 (the smallest complex particles, collected from the top of 2:1 suspension prepared in ethanol, see entry 12 in Table 1); b) TGA and DTG curves of the same complex. In case of pure melamine, the complete single-step weight loss is due to sublimation of the material.

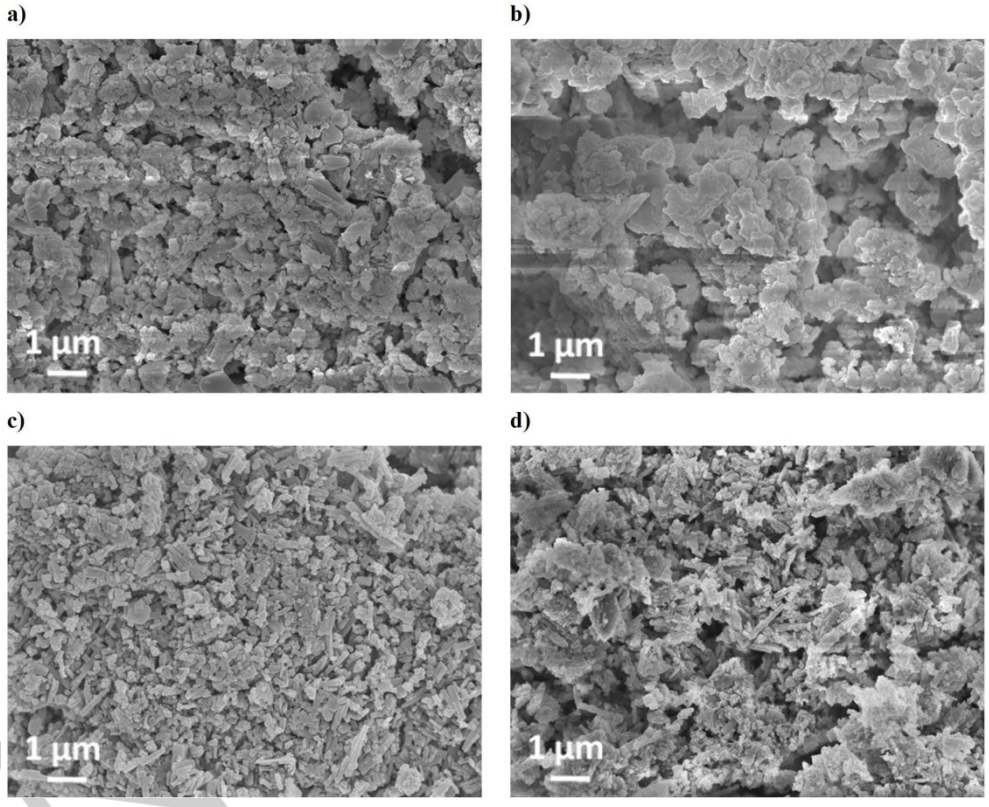

Figure S3. SEM images of starting complexes (a, c) (in text they are referred to as 3:1 and 6:1) and the intermediates obtained by heating these starting complexes to 270 °C (b, d).

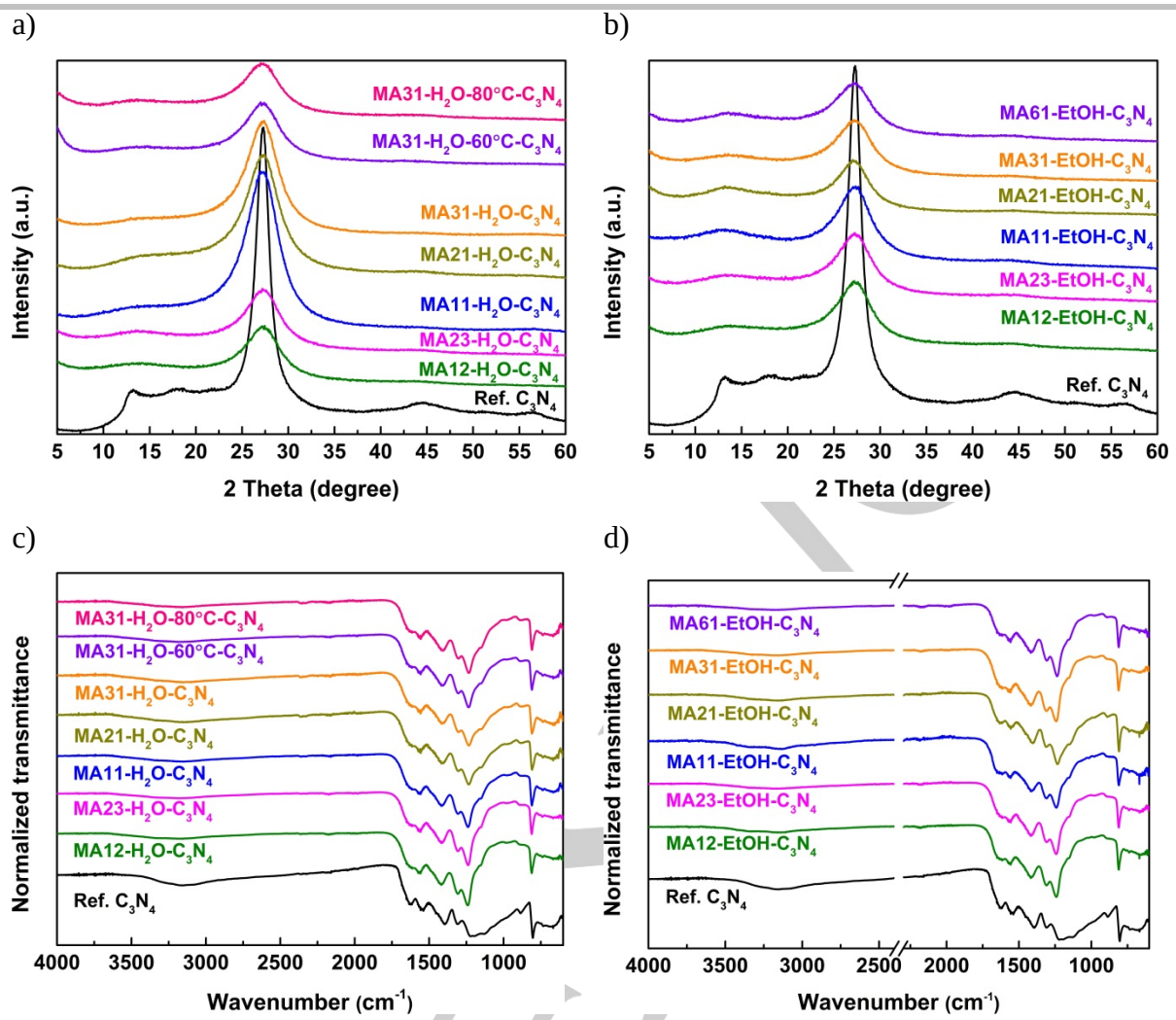

Figure S4. PXRD patterns and FTIR spectra of MAxy-S-C_3N_4 obtained by heating up the MAxy-complexes prepared in water (a, c) and ethanol (b, d) and of reference carbon nitride. Here, *x* and *y* indicate the molar ratio between melamine and $Al(NO_3)_3 \cdot 9H_2O$ used to prepare the starting complex, and S indicates the solvent.

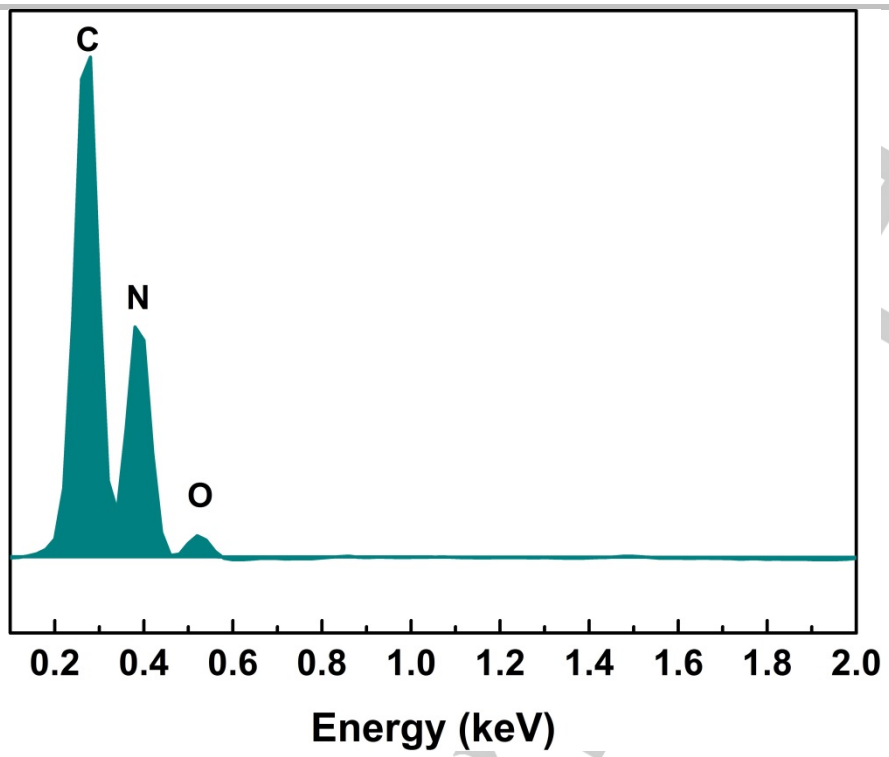

Figure S5. The energy dispersive X-ray spectroscopy (EDX) spectrum of MA23-EtOH-C_3N_4.

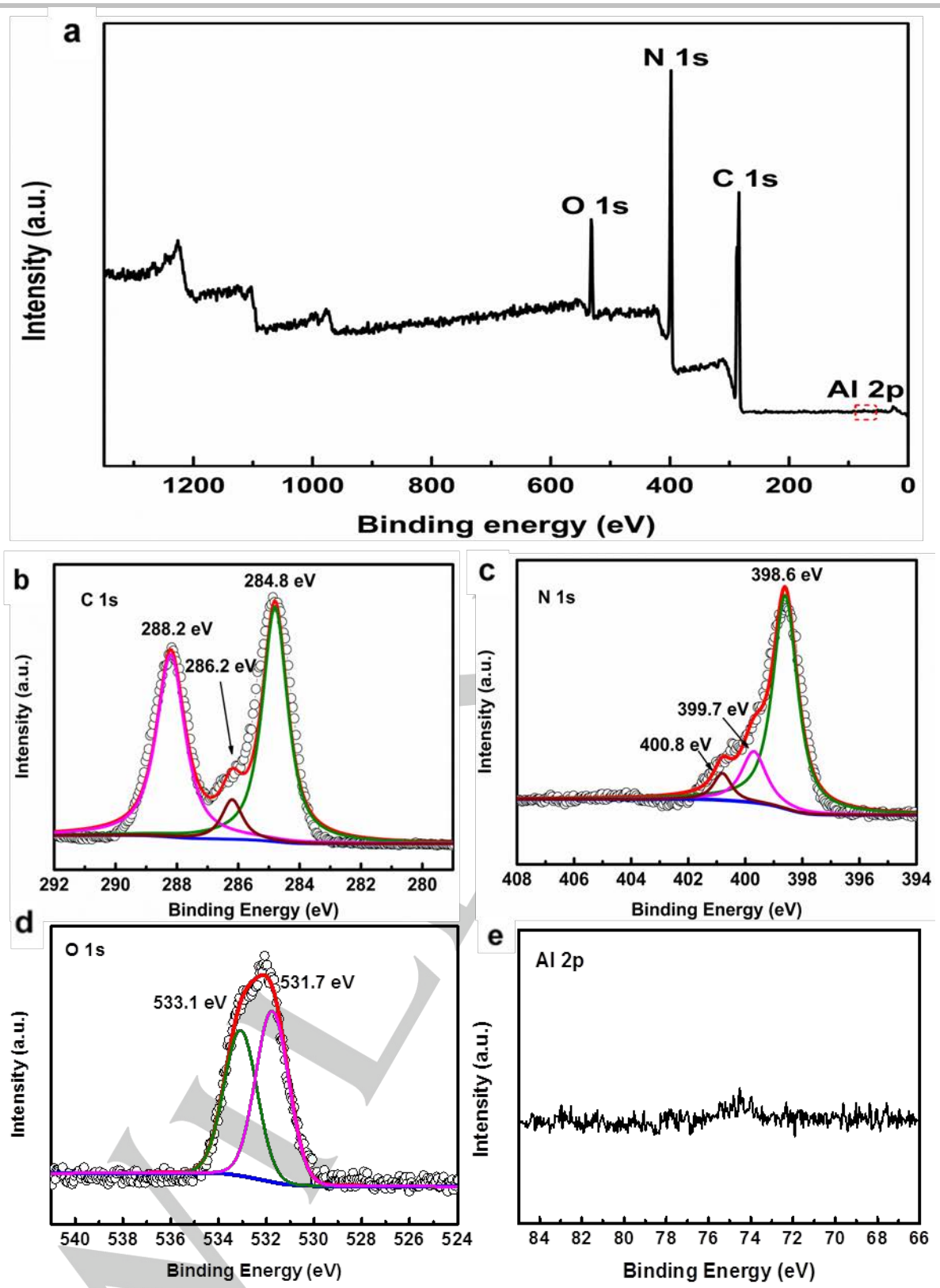

Figure S6. a) Survey, b) C1s, c) N1s, d) O1s, and e) Al2p XPS spectra of MA23-EtOH-C_3N_4 product.

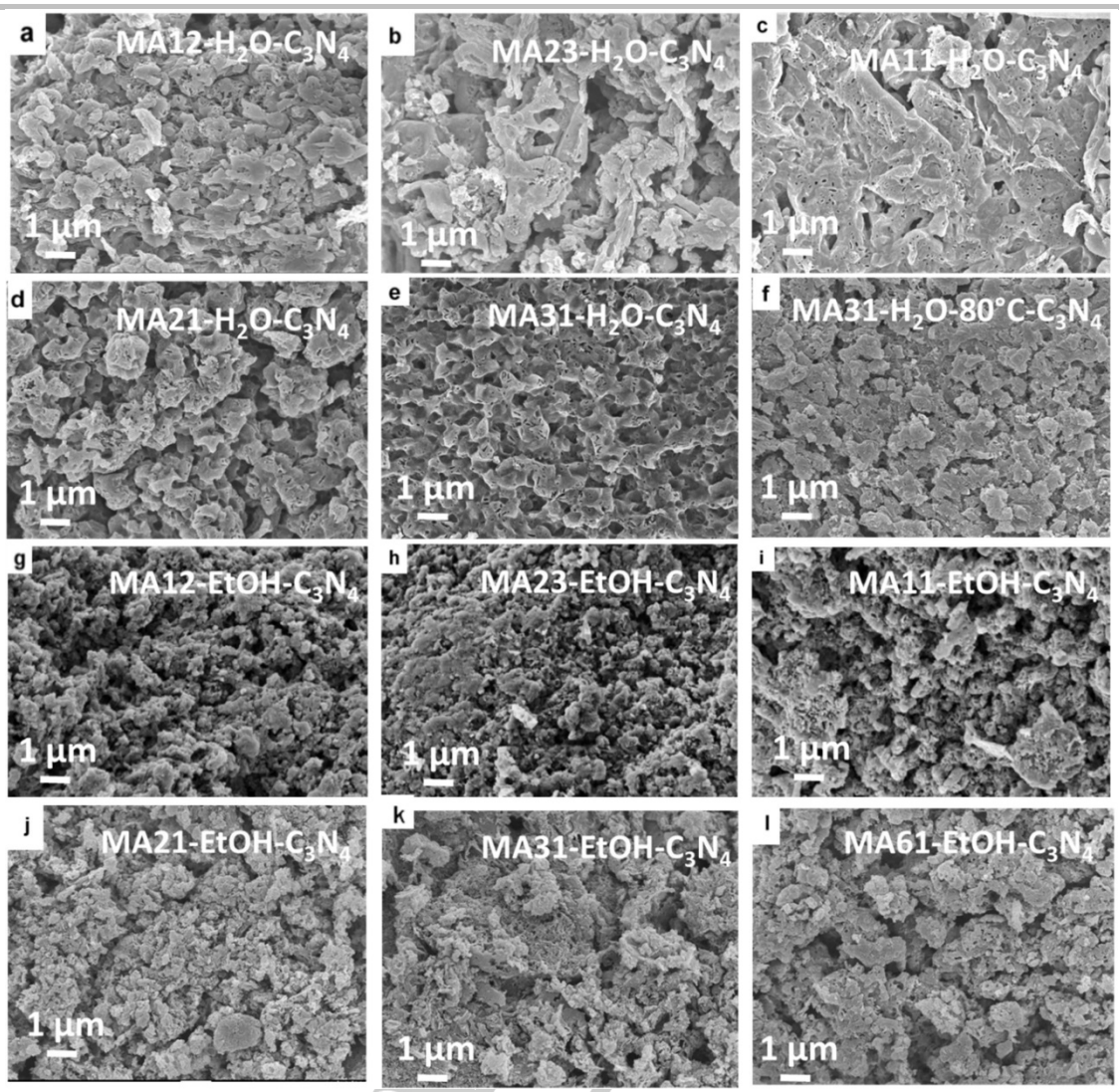

Figure S7. Representative SEM images of carbon nitrides derived from MAxy-complexes.

Table S2. Band gap values, BET surface areas, porosity description and RhB degradation activity of MA-derived products and reference carbon nitrides.

Entry	Product name	Band gap eV	BET s.a., m^2/g	Pore diameter, nm	Pore volume, cc/g	K, $*10^{-3}$/min WLED	K, $*10^{-3}$/min 465nm
1	g-C_3N_4	2.74	9.5	2.8	0.01	3.68	4.47
2	CM-C_3N_4	n/a	n/a	n/a	n/a	21.7	12.3
3	MA12-H_2O-C_3N_4	2.93	37.5	3.2	0.07	48.8	n/a
4	MA23-H_2O-C_3N_4	2.91	29.7	2.8	0.06	36.3	n/a
5	MA11-H_2O-C_3N_4	2.90	19.4	2.8	0.02	30.7	n/a
6	MA21-H_2O-C_3N_4	2.85	16.9	2.8	0.03	14.6	n/a
7	MA31-H_2O-C_3N_4	2.86	13.3	4.2	0.02	16.0	n/a
8	MA31-H_2O-60°C-C_3N_4	n/a	20.9	3.8	0.04	18.9	n/a
9	MA31-H_2O-80°C-C_3N_4	n/a	33.8	4.2	0.08	23.7	n/a
10	MA31-H_2O-gel-C_3N_4	2.93	50.8	4.2	0.10	52.2	n/a
11	MA12-EtOH-C_3N_4	2.91	44.3	2.8	0.08	n/a	19.8
12	MA23-EtOH-C_3N_4	2.93	44.3	3.2	0.12	n/a	26.1
13	MA11-EtOH-C_3N_4	2.91	20.5	2.8	0.01	n/a	17.7
14	MA21-EtOH-C_3N_4	2.93	55.9	2.9	0.15	59.1	36.4
15	MA31-EtOH-C_3N_4	2.90	34.9	1.7	0.08	71.6	25.2
16	MA61-EtOH-C_3N_4	2.89	20.1	3.8	0.07	58.1	n/a
17	MA21-EtOH-top-C_3N_4	n/a	57.8	13.9	0.19	63.6	n/a
18	MA31-EtOH-top-C_3N_4	n/a	89.2	16.7	0.26	57.9	n/a
19	MA61-EtOH-top-C_3N_4	n/a	52.1	4.9	0.11	81.7	n/a

n/a - not analyzed

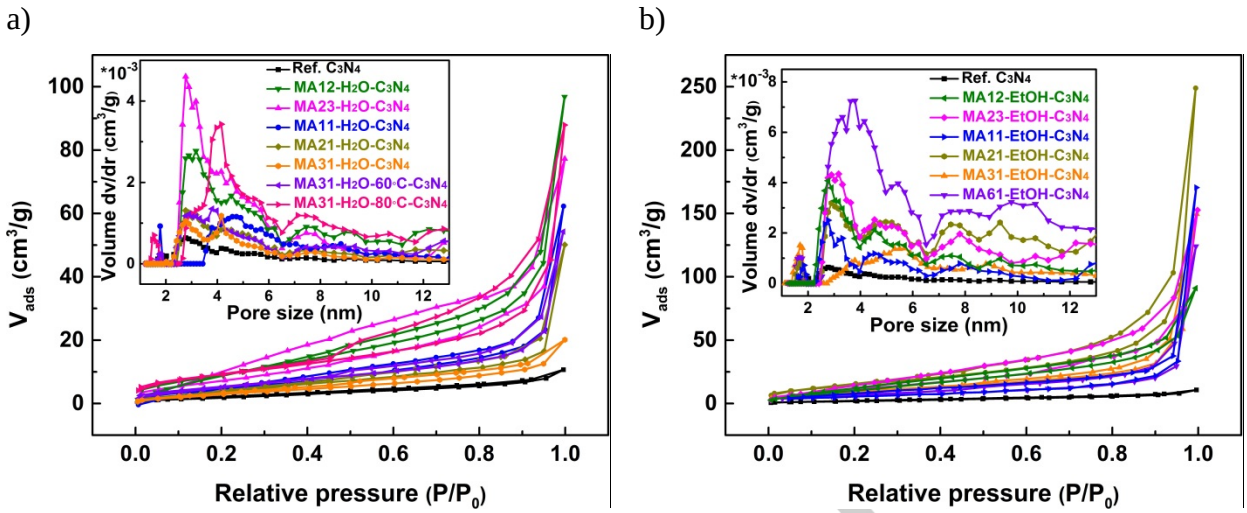

Figure S8. Nitrogen adsorption–desorption isotherms of MAxy-H_2O-C_3N_4 (a) and MAxy-EtOH-C_3N_4 (b) and bulk g-C_3N_4. Insets are pore size distributions calculated by the nonlocal density functional theory method (NLDFT).

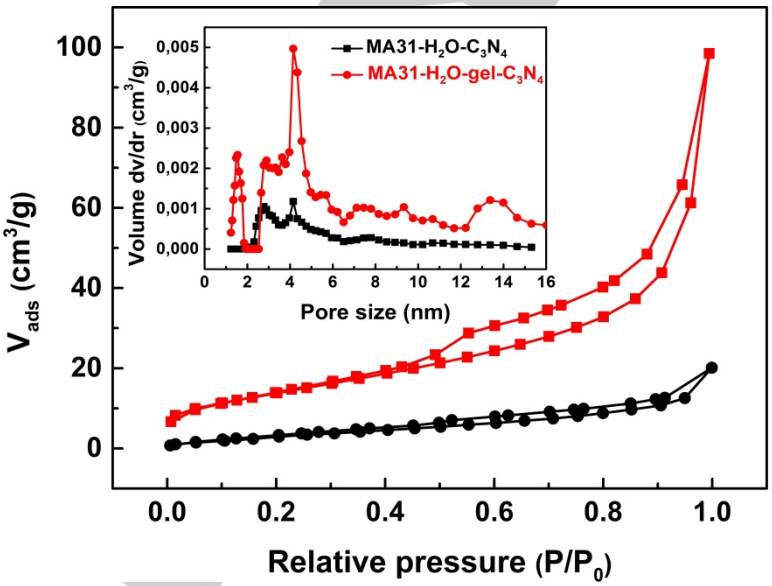

Figure S9. Comparison of nitrogen adsorption–desorption isotherms and the corresponding pore size distributions for carbon nitrides prepared by direct heating MA31-H_2O gel and the one obtained from the dried gel.

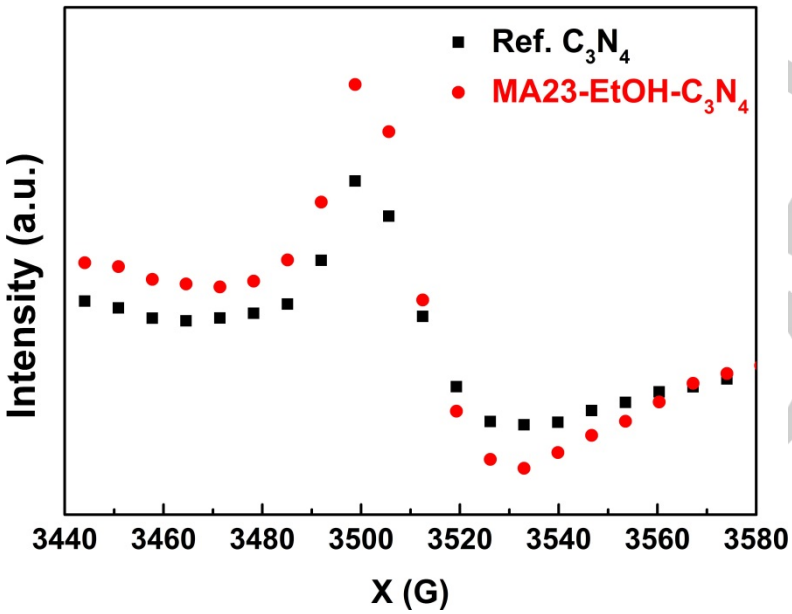

Figure S10. Room temperature EPR spectra of MA23-EtOH-C_3N_4 and bulk g-C_3N_4.

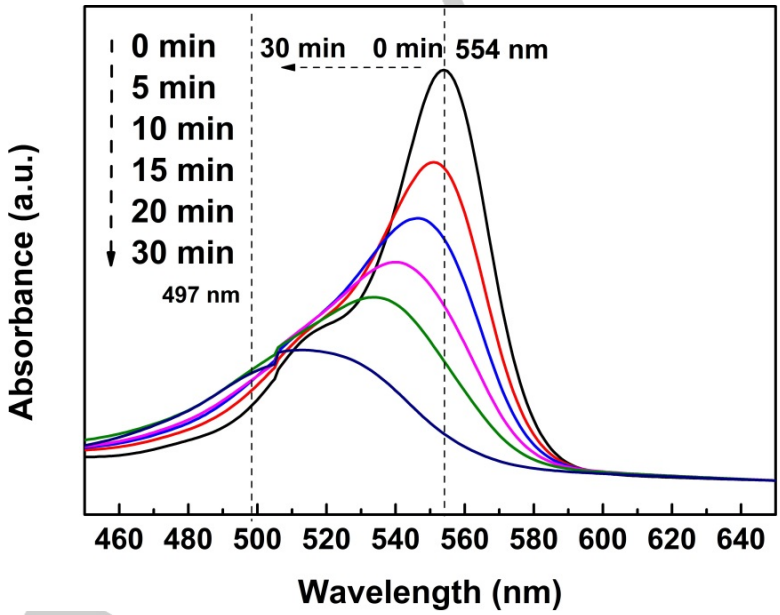

Figure S11. UV-vis absorption spectra of RhB aqueous solutions containing MA61-EtOH-top-C_3N_4 catalyst as a function of irradiation time.

a) b)

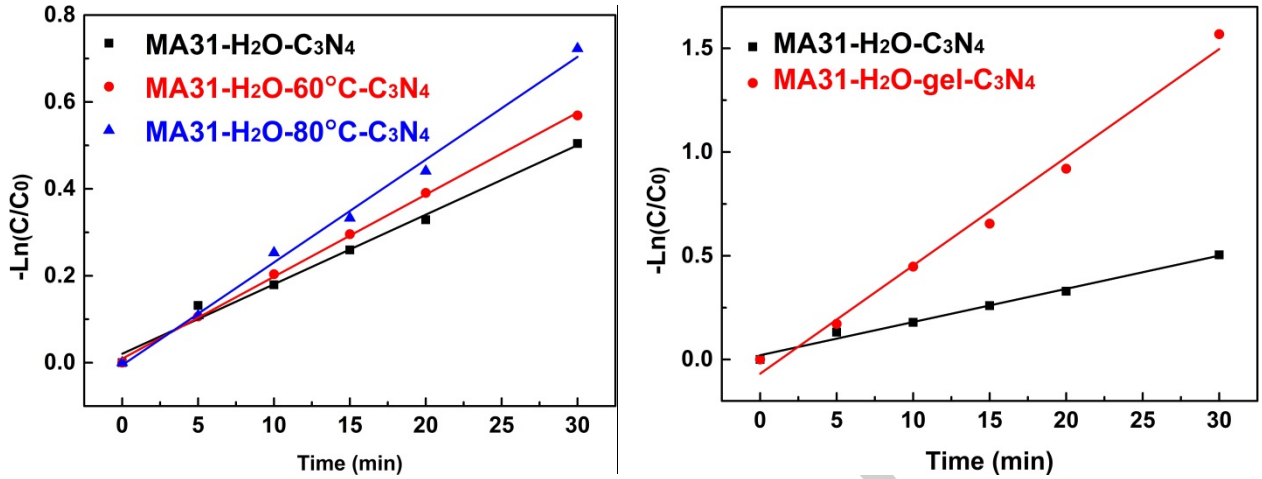

Figure S12. (a) RhB degradation activity of MA31-H_2O gels prepared at different conditions; gels prepared at higher temperatures are characterized by better complex stoichiometry; (b) comparison of RhB degradation activity of carbon nitride prepared by direct heating MA31-H_2O gel and the one obtained from dried gel.

a) b)

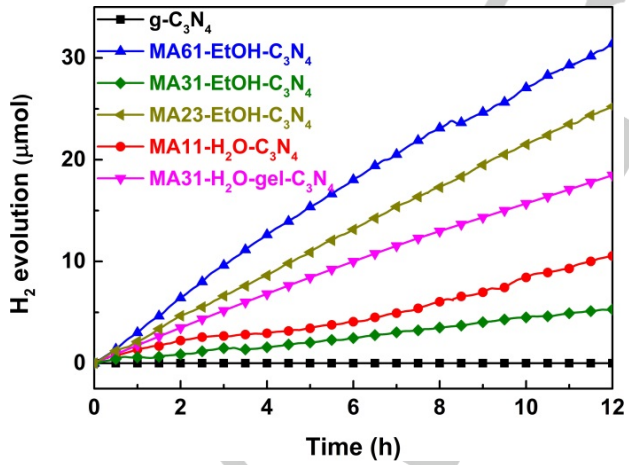

Product	H_2 evolution rate, μmol/h
g-C_3N_4	< 0.25
MA61-EtOH-C_3N_4	2.62
MA31-EtOH-C_3N_4	0.44
MA23-EtOH-C_3N_4	2.10
MA11-H_2O-C_3N_4	0.88
MA31-H_2O-gel-C_3N_4	1.54

Figure S13. (a) Time course of H_2 production upon irradiation with white light (50W LED array) in the presence of different photocatalysts; (b) estimated hydrogen evolution rates.

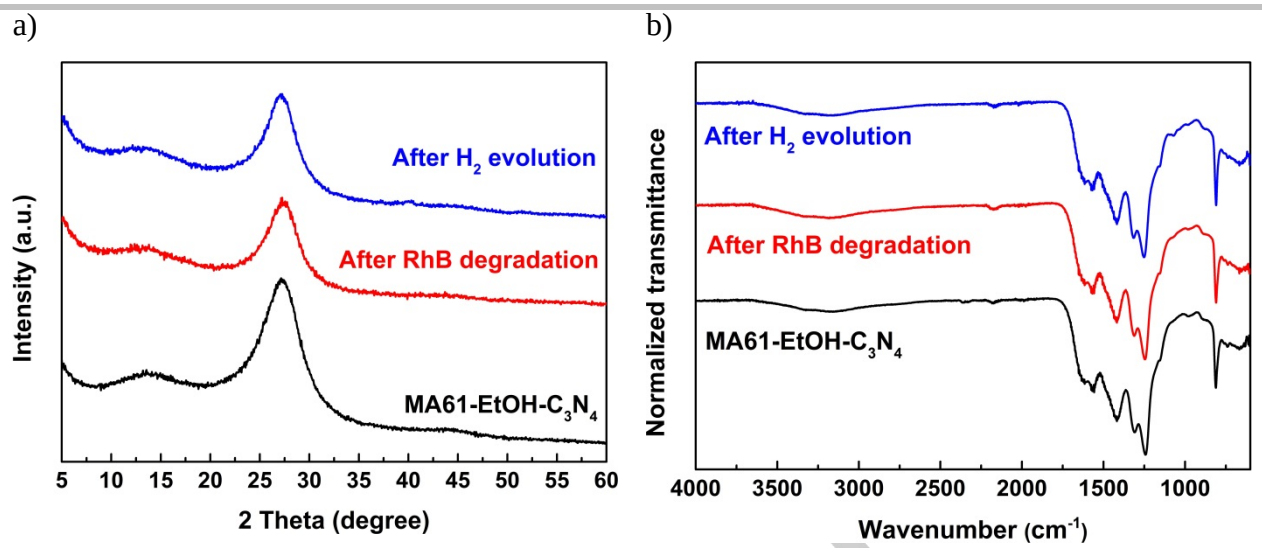

Figure S14. PXRD patterns (a) and FTIR spectra (b) of MA61-EtOH-C_3N_4 before and after RhB photodegradation/H_2 evolution experiments.

[S1] Schwarze, M.; Stellmach, D.; Schroder, M.; Kailasam, K.; Reske, R.; Thomas, A.; Schomacker, R., Quantification of photocatalytic hydrogen evolution. *Physical Chemistry Chemical Physics* **2013,** 15, (10), 3466-3472.